The all-seeing eye of resonant Auger electron spectroscopy: a study on aqueous KCl

Tsveta Miteva,[*,†] Nikolai V. Kryzhevoi,[‡] Nicolas Sisourat,[†] Christophe Nicolas,[¶] Wandared Pokapanich,[§] Thanit Saisopa,[‖] Prayoon Songsiriritthigul,[‖] Yuttakarn Rattanachai,[⊥] Andreas Dreuw,[#] Jan Wenzel,[#] Jérôme Palaudoux,[†] Gunnar Öhrwall,[@] Ralph Püttner,[△] Lorenz S. Cederbaum,[‡] Jean-Pascal Rueff,[†,¶] and Denis Céolin[*,¶]

†*Sorbonne Université, CNRS, Laboratoire de Chimie Physique Matière et Rayonnement, UMR 7614, F-75005 Paris, France*

‡*Theoretische Chemie, Physikalisch-Chemisches Institut, Universität Heidelberg, Im Neuenheimer Feld 229, D-69120 Heidelberg, Germany*

¶*Synchrotron SOLEIL, l'Orme des Merisiers, Saint-Aubin, F-91192 Gif-sur-Yvette Cedex, France*

§*Faculty of Science, Nakhon Phanom University, Nakhon Phanom 48000, Thailand*

‖*School of Physics, Suranaree University of Technology, Nakhon Ratchasima 30000, Thailand*

⊥*Department of Applied Physics, Faculty of Sciences and Liberal Arts, Rajamangala University of Technology Isan, Nakhon Ratchasima 30000, Thailand*

#*Interdisciplinary Center for Scientific Computing, Ruprecht-Karls University, Im Neuenheimer Feld 205A, D-69120 Heidelberg, Germany*

@*MAX IV Laboratory, Lund University, P.O. Box 118, SE-22100 Lund, Sweden*

△*Fachbereich Physik, Freie Universität Berlin, Arnimallee 14, D-14195, Berlin, Germany*

E-mail: tsveta.miteva@upmc.fr; denis.ceolin@synchrotron-soleil.fr

Abstract

X-ray absorption and Auger electron spectroscopies are powerful tools to probe the electronic structure and immediate surroundings of ions in solution. In this work we use a combination of these methods to study the electronic structure and decay of aqueous KCl at the K-edges of K^+ and Cl^-. Although the two ions are isoelectronic, their Auger electron spectra as a function of the photon energy exhibit notably different features. These features are a result of the excitation and Auger decay of the dipole forbidden states in aqueous K^+, which become dipole allowed due to mixing with the closely lying bright states in the presence of the solvent. The results of this work confirm the sensitivity of core level spectroscopies to the electronic structure of solvated species and represent a pioneering study of the decay processes initiated by photoabsorption in the tender x-ray regime close to threshold in liquids.

Graphical TOC Entry

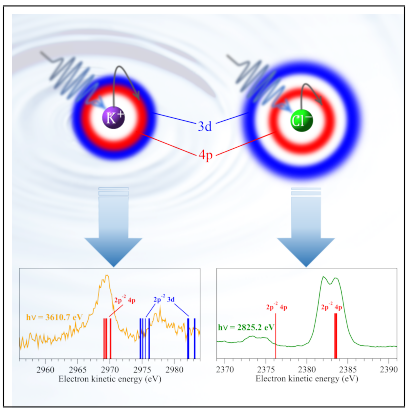

Keywords

Solvated ions, Auger electron spectroscopy, x-ray absorption spectroscopy

X-ray absorption (XAS) and Auger electron spectroscopies (AES) are powerful tools to study the electronic structure and the nearest environment of atoms and molecules in gas, liquid and solid phase. Understanding how atoms or molecules respond to irradiation with x-rays gives insight into the structure of solutions (Ref.[1] and references therein), and the mechanisms of radiation damage[2–4]. Upon absorption of an x-ray photon, either core excited or core ionized states of a specific atom are populated depending on the photon energy. The relaxation of these highly energetic states involves an ultrafast cascade of intraatomic processes, such as radiative and Auger decays, and it depends on the character of the initially populated states[5–12]. Furthermore, if the initially excited or ionized species is embedded in an environment, interatomic processes are possible[4,13–16].

In a solution, the course of such electronic decay cascades initiated by x-ray photoabsorption differs from that in atomic and molecular clusters due to the shorter distances and stronger interatomic interactions. In this work we used AES together with XAS in the tender x-ray regime to study the electronic decay processes following x-ray absorption of aqueous potassium chloride at the K-edges of both K^+ and Cl^-. In particular, we demonstrate experimentally that at photon energies below the K-edges of the two ions, core excited states are populated. These states undergo resonant Auger decay within less than 1 fs. Although the K^+ and Cl^- ions are isoelectronic, they have different fingerprints in the resonant Auger spectra. We demonstrate that these differences result from different electronic structures of the two ions, thus confirming that the combination of XAS and AES techniques is a sensitive probe of the electronic structure of solutions.

The resonant and normal Auger processes which we investigated in this work are schematically shown on Fig. 1. The $KL_{2,3}L_{2,3}$ normal Auger decay following K-shell ionization of aqueous K^+ and Cl^- populates the $2p^{-2}(^3P, ^1D, ^1S)$ final states. The ^3P final states have a very low intensity since the corresponding transitions are forbidden from angular momentum and parity conservation rules. In the case of K^+_{aq} the maxima of the ^1S and ^1D $KL_{2,3}L_{2,3}$ Auger lines at photon energy $h\nu = 3616.0$ eV are located at 2958.0 eV and 2968.5 eV kinetic

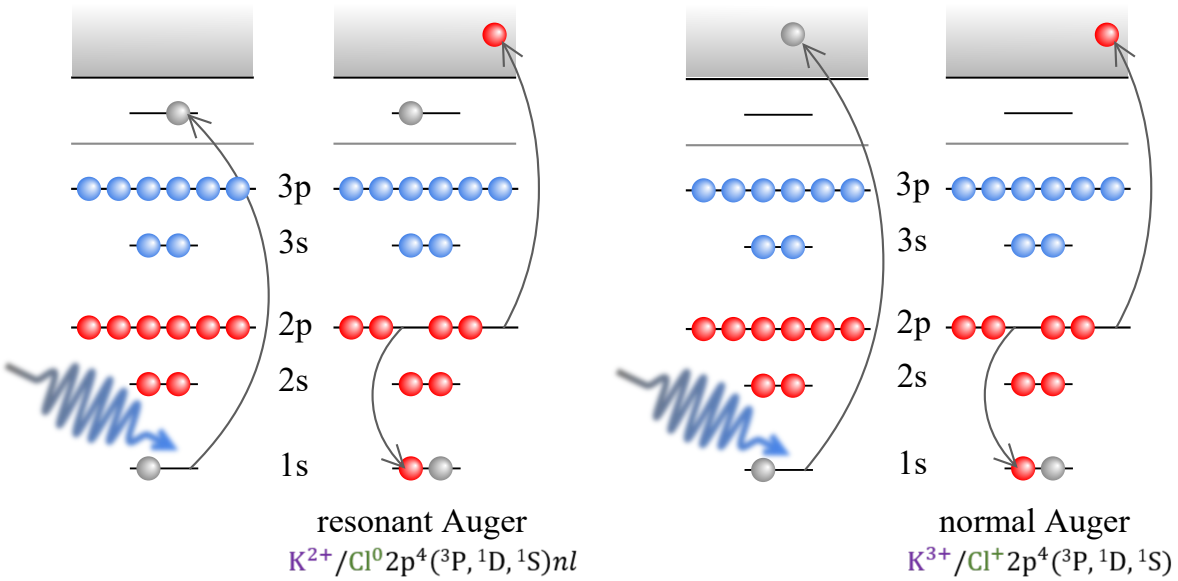

Figure 1: Schematic representation of the resonant (left) and normal (right) Auger processes of the isoelectronic K^+ and Cl^- ions.

energy, respectively (Fig. 2(a)). For Cl^-_{aq}, the lines corresponding to the Cl^+ $2p^{-2}(^1S)$ and (^1D) states are located at 2373.1 eV and 2382.0 eV kinetic energy for a photon energy of 2830.0 eV (Fig. 3).

The $KL_{2,3}L_{2,3}$ normal Auger lines may be shifted to higher kinetic energies and also disperse with photon energy close to threshold due to energy exchange between the photoelectron and Auger electron called post-collision interaction (PCI)[17,18]. The effect of dispersion of the electron energy is manifested as an asymmetric tail of the main peaks at photon energies 3616 eV in the case of K^+, and 2830 eV in the case of Cl^-. In order to estimate the PCI shift, we compare the positions of the normal KLL Auger lines of both Cl^-_{aq} and K^+_{aq} close to threshold with those recorded far from threshold, at photon energies $h\nu = 5$ keV[16]. We observe a shift of $\sim$1 eV of the maxima towards lower kinetic energies as compared to the spectra reported in[16]. The magnitude of the shift is constant in the photon energy range of $\sim$8 eV above threshold and similar for the two ions. A possible explanation of the shift observed in our experiment is given in Ref.[19] where it was proposed that it is a result of a process of internal ionization, i.e. excitation of the photoelectron into the conduction band,

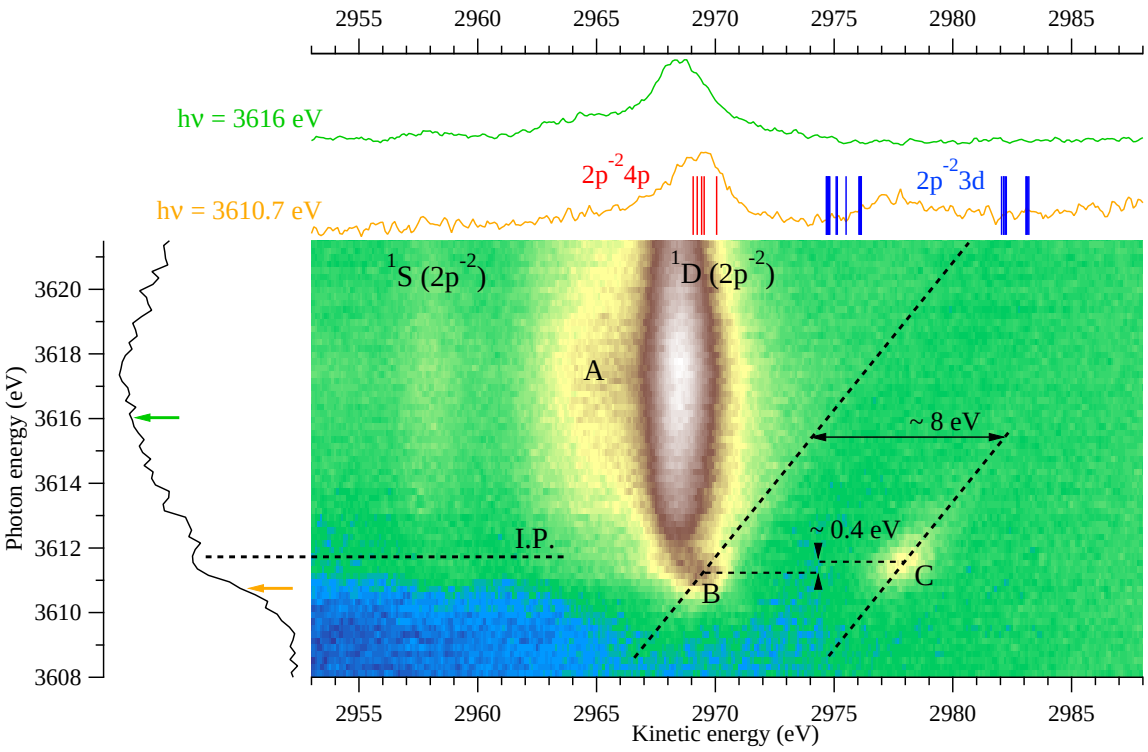

Figure 2: (a) 2D map showing the kinetic energy of the electrons emitted in $KL_{2,3}L_{2,3}$ Auger decay vs the photon energy in the vicinity of the K-edge of aqueous K^+. The features A, B and C are discussed in the text. (b) experimental partial electron yield spectrum of K^+ obtained after integrating over the kinetic energies of the Auger electrons. (c) Auger spectra at photon energies 3610.7 eV and 3616 eV. The vertical bars in the resonant Auger spectrum measured at 3610.7 eV indicate the energy positions of the theoretical doublet $2p^{-2}$ 3d (blue) and $2p^{-2}4p$ (red) states of $K^+(H_2O)_6$.

followed by normal Auger decay. The observed shift was explained as resulting from the PCI-like interaction between the Auger electron and the electron excited to the conduction band.

Finally, the normal Auger ^{1}D main line of K^+ differs from that of Cl^- by the presence of a large shoulder on the low kinetic energy side at about 2965 eV kinetic energy, feature A (Fig. 2). This shoulder is attributed to electron transfer from the solvent water molecules to the unoccupied 3d orbitals of K^+ [16]. In the case of Cl^-, there is no experimental evidence of such intense electron transfer processes.

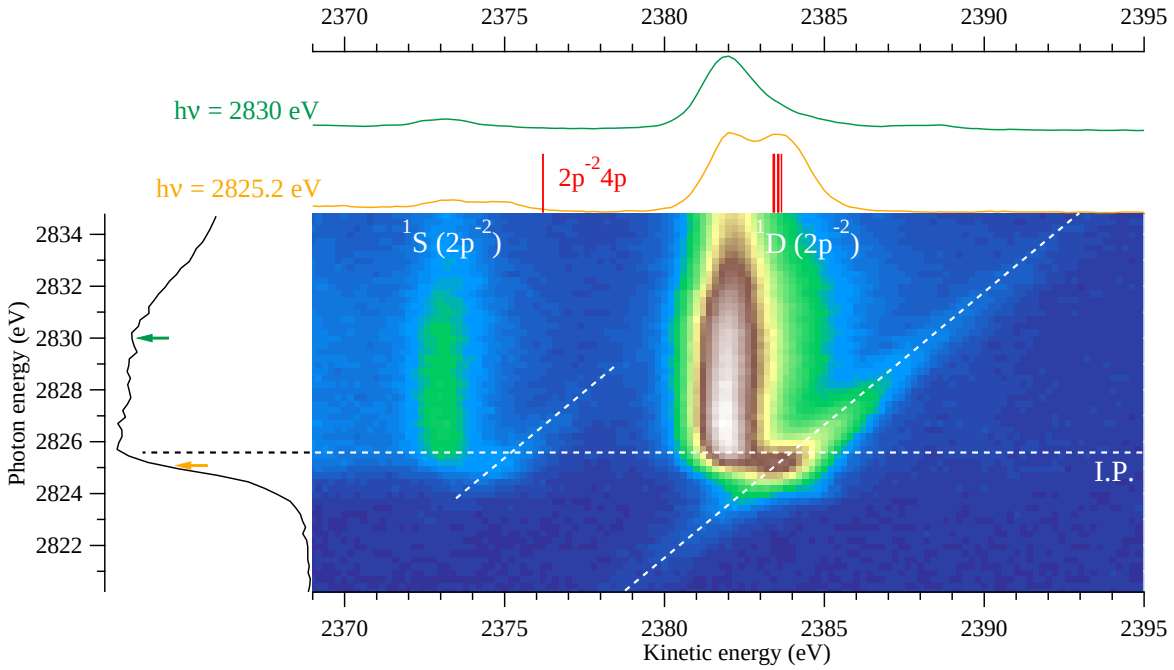

Figure 3: (a) 2D map showing the kinetic energy of the electrons emitted in $KL_{2,3}L_{2,3}$ Auger decay vs the photon energy in the vicinity of the K-edge of aqueous Cl^-. (b) experimental partial electron yield spectrum of Cl^- obtained after integrating over the kinetic energies of the Auger electrons. (c) Auger spectra at photon energies 2825.2 eV and 2830.0 eV. The vertical bars in the resonant Auger spectrum at 2825.2 eV indicate the energy positions of the theoretical doublet $2p^{-2}4p$ states of $Cl^-(H_2O)_6$.

The $KL_{2,3}L_{2,3}$ Auger decay following resonant K-shell excitation of solvated K^+ and Cl^- is schematically presented on Fig. 1. The pre-edge regions of the XAS spectra of K^+ and Cl^- do not exhibit any high intensity peaks owing to the lifetime broadening and energetic proximity of the core excited states to the ionization threshold (Figs. 2 and 3). Consequently, solely from these spectra, one cannot conclude whether there are core excited states in the pre-edge structure. Instead these states have to be identified by their resonant Auger features, which differ from the normal Auger features of core ionized states. Thus, for Cl^-, the lowest core excited state is located at 2825.2 eV, which is in good agreement with the position of the Cl^- $1s^{-1}4p$ excitation determined from Cl K-edge XAS experiments[20,21]. In the case of K^+, there are two dispersive features with maxima at photon energies of 3611.2 eV (B) and

3611.6 eV (C). The positions of these two core excited states are close to the energy of the $1s^{-1}4p$ excitation in bare K^+ at 3610.7 eV[22].

The resonant Auger features produced in the decay of these core excited states are quite different for Cl^- and K^+. In the 2D map of Cl^- shown in Fig. 3 there are two dispersive features indicated with diagonal dashed lines. The maxima of these features are at 2825.2 eV photon energy and 2374.6 and 2383.4 eV kinetic energy, respectively. In the case of K^+, the dispersive line related to the ^1S main line cannot be clearly identified due to the presence of strong background. Instead two dispersive features related to the ^1D main line are observed denoted as B and C on Fig. 2. Feature B exhibits a maximum at $h\nu = 3611.2$ eV and 2969.2 eV kinetic energy. The additional feature C appears at $h\nu = 3611.6$ eV and 2978.1 eV kinetic energy, thus it is separated by approximately 400 meV in photon energy and 8.3 eV in kinetic energy from the maximum of feature B.

In order to rationalize the pre-edge region of the experimental XAS spectra and the differences in the AES spectra of K^+_{aq} and Cl^-_{aq}, we computed the lowest core excited states of the bare K^+ and Cl^- ions and their hexa-coordinated clusters (Fig. 4). The lowest bright peak in the XAS spectra of the bare ions corresponds to the dipole allowed $1s^{-1}4p$ state followed by the second bright state, $1s^{-1}5p$, which is located 4.3 eV and 10.8 eV higher in K^+ and Cl^-, respectively. We also show the dipole forbidden $1s^{-1}3d$ states of the bare ions as blue crosses. It is noteworthy that the positions of the $1s^{-1}4p$ and $1s^{-1}3d$ states are inverted in K^+ and Cl^-, and moreover, the splitting between these states is about two times smaller in K^+, which as explained later is crucial for understanding the Auger spectra of the two ions. Upon addition of water molecules, the degeneracy of the states is lifted, and moreover, they interact with other states of the ion or the neighboring water molecules (Fig. 4(a),(b)). Thus, dipole forbidden states acquire intensity in the cluster. A similar effect was observed in the XAS spectra of microsolvated clusters of Na^+ and Mg^{2+}[23].

Further by comparison of the experimental and theoretical XAS spectra, we assume that only the lowest peak in the theoretical XAS spectra is populated in the experiment. In

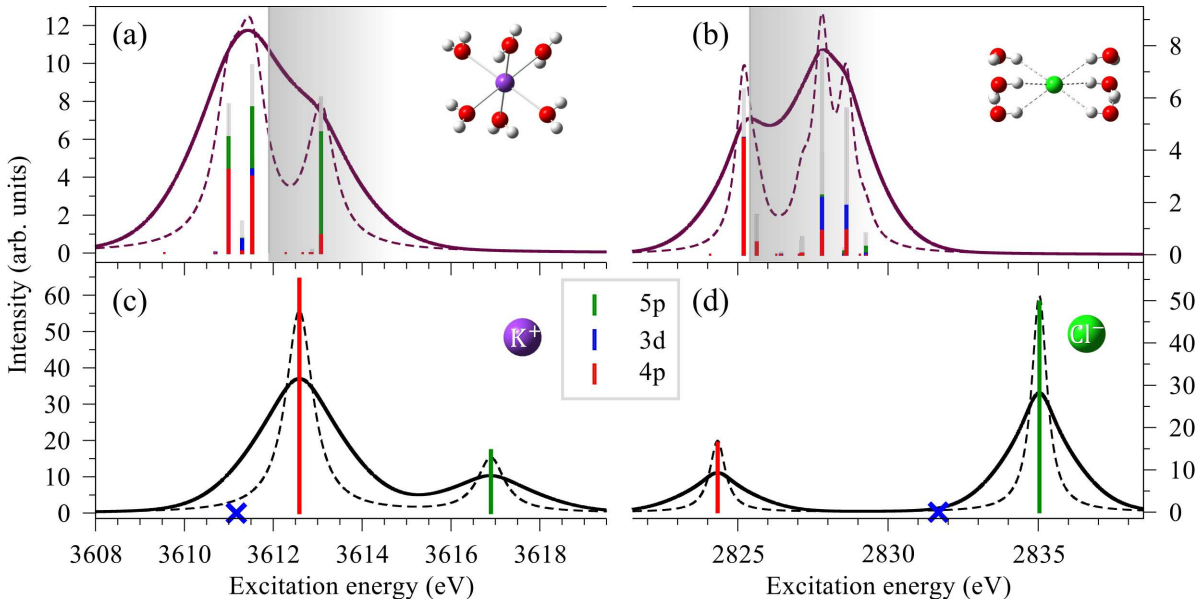

Figure 4: XAS spectra of the lowest K-shell resonant transitions in the bare K^+ (c) and Cl^- (d) ions and their 6-coordinated clusters ((a) and (b)). For comparison with the experiment, the theoretical stick spectra are convolved with a Lorentzian of FWHM 0.74 eV and 0.62 eV in the case of K^+ and Cl^- [44] (dashed line)and a Voigt profile (solid line). The stick spectrum corresponds to the projections of the SONOs corresponding to the core excited states of the 6-coordinated clusters on the basis of SONOs corresponding to the $1s^{-1}3d$, $1s^{-1}4p$, and $1s^{-1}5p$ states of the bare ions. The remaining contributions from higher-lying atomic core excitations or from excitations to the solvent molecules are depicted as grey sticks. The theoretical XAS spectra of both K^+ and Cl^- were shifted to higher photon energies such that the energies of the lowest core excited states correspond to the experimentally determined ones. The experimental ionization thresholds are depicted as grey boxes.

the 6-coordinated K^+ cluster the lowest peak in the spectrum contains three states. The lowest and highest lying states are split by approximately 0.5 eV and they have mixed 4p and 5p character. The low intensity state lying between these two states has a predominantly $1s^{-1}3d$ character. Since the dispersive feature B appears at low excitation energies, we assume that it is produced in the resonant Auger decay of the lowest core excited states of K^+ of predominantly $1s^{-1}4p$ character. Moreover, we can attribute the feature C to the resonant Auger decay of the low intensity dipole forbidden $1s^{-1}3d$ state. Thus, we explain both the energy splitting of ∼400 meV photon energy of B and C, and the fact that island C has lower intensity than B (Fig. 2). In the hexa-coordinated cluster of Cl^-, the solvent molecules have little influence on the position and character of the first state – it has mainly

Cl^- $1s^{-1}4p$ character with some admixture of states of the nearest water molecules. We therefore attribute the two dispersive features associated with the ^1S and ^1D main lines on the 2D map of Cl^- to the resonant Auger decay of this core excited state involving mostly the 4p orbitals of chloride.

To fully characterize the dispersive features on the experimental 2D maps, we also computed the lowest $K^{2+}[2p^{-2}nl](H_2O)_6$ and $Cl^0[2p^{-2}nl](H_2O)_6$ doublet states corresponding to the lowest final spectator resonant Auger states. The energy positions of these lines are shown as bars in the upper panels of Figs. 2 and 3. In both cases, the lowest $2p^{-2}(^1D)4p$ states were shifted such that the kinetic energies coincide with the maxima of the dispersive features on the high kinetic energy part of the ^1D main line.

As mentioned above, we attribute the island B on the 2D map of K^+_{aq} to the decay of the lowest lying core excited state of predominantly $1s^{-1}4p$ character. Supposing that this state undergoes mostly pure spectator resonant Auger decay as in the isoelectronic Ar atom[24], then the lowest $2p^{-2}4p$ states are populated resulting in Auger electrons of between 2969.0 and 2970.5 eV kinetic energy. As can be seen from the Auger spectrum at $h\nu = 3610.7$ eV (upper panel of Fig. 2), the lowest $2p^{-2}4p$ states of $K^+(H_2O)_6$ are separated by $\sim$5 and 12-13 eV from two higher lying groups of $2p^{-2}3d$ states. Thus, the group of $2p^{-2}3d$ states at $\sim$2975 eV lies closer to the position of island C. Consequently, we attribute this dispersive feature as originating from the resonant Auger decay of the $1s^{-1}3d$ excitation to the group of $2p^{-2}3d$ states. The splitting between the $2p^{-2}4p$ and $2p^{-2}3d$ states in our calculation is smaller than the splitting between the islands B and C most probably because we do not theoretically account for the effect of distant solvent shells. Concerning the $2p^{-2}3d$ states at kinetic energies between 2982 and 2983 eV, we conclude that they are not populated via the Auger process since no additional experimental features are observed.

Another argument in favor of the $2p^{-2}3d$ character of the feature C is the energy difference between the spectral features A and C. Feature A originates from electron transfer processes from water molecules (W) to the doubly core ionized potassium ion and has the

configuration $K^{2+}(2p^{-2}3d)W^{-1}$. The lowest ionization potential of liquid water is about 11.16 eV[25] which fits well with the observed A-C splitting. Based on the above energetic arguments we attribute the island C as originating from resonant Auger decay to the K^{2+} $2p^{-2}3d$ final state.

In the computed $Cl^0[2p^{-2}nl](H_2O)_6$ spectrum there are two groups of states split by about 7 eV (upper panel of Fig. 3). The lower kinetic energy group corresponds to the $2p^{-2}(^1S)4p$ final states, whereas the higher kinetic energy group corresponds to the $2p^{-2}(^1D)4p$ final states. The splitting between these two groups is in good agreement with the experimental splitting between the dispersive features on the high kinetic energy sides of the ^1S and ^1D main peaks. Consequently, we attribute these dispersive features as resulting from the resonant Auger decay of the $1s^{-1}4p$ core excited state of Cl^-_{aq} to the $2p^{-2}(^1S)4p$ and $2p^{-2}(^1D)4p$ final states.

In summary, we studied the electronic structure of aqueous solution of KCl at the K-edges of both K^+_{aq} and Cl^-_{aq} using a combination of x-ray absorption and Auger electron spectroscopy in the tender x-ray regime, and *ab initio* calculations. The Auger electron spectra of both ions exhibit features of normal and resonant Auger processes. The latter process proceeds differently for aqueous K^+ and Cl^- due to the population of the dipole forbidden K^+ $1s^{-1}3d$ state in a solution. The spectator Auger decay of this state produces an additional dispersive feature which is manifested as a separate peak in the Auger electron spectrum. In the case of Cl^- only fingerprints of the population and Auger decay of the dipole allowed $1s^{-1}4p$ excitation are observed in the spectrum.

The reported results are an important first step in the study of the chains of relaxation steps triggered by photoabsorption in the tender x-ray regime. The Auger processes considered here are inevitably followed by multiple intra- and interatomic electronic decays, such as interatomic Coulombic decay (ICD) and electron-transfer mediated decay (ETMD). As a result of the latter processes, genotoxic free radicals and slow electrons are formed in the vicinity of the metal center. The magnitude of the damage inflicted upon the environment

and the energies of the emitted electrons depend on the initial Auger step, and can therefore be controlled by tuning the energy of the radiation. Consequently, the results of this work can have implications in understanding radiation chemistry and radiation damage in biologically relevant systems.

Methods

Experimental

For the present experiment we used the newly operational microjet setup that was specifically designed for the HAXPES station of the GALAXIES beamline[26,27]. The aqueous potassium chloride solution was prepared by mixing >99% KCl salt with deionized water. Filtering and degazing procedures were systematically performed before injecting the solution. The spectrometer resolution of about 0.6 eV was achieved with the 500 eV pass energy and 0.5 mm slits. The photon energy resolution achieved at 2.8 keV and 3.6 keV was about 0.3 eV and 0.4 eV, respectively. The experimental 2D maps representing the evolution of the KLL Auger spectra in the vicinity of the $Cl^-$and K^+ K-edges, as a function of the photon energy, are shown in Figs. 2 and 3, respectively. The aqueous K^+ and Cl^- 1s ionization potentials were measured at hν=5keV and calibrated on the liquid contribution of the O1s XPS spectrum.[28] The maps were also calibrated using the O1s photoelectron line of liquid water but at photon energies close to the potassium and chloride 1s ionization thresholds.

Ab initio calculations

The theoretical X-ray absorption spectra were computed for the hexa-coordinated clusters of both ions, $K^+(H_2O)_6$ and $Cl^-(H_2O)_6$, which can be considered as representatives of the complete first solvation shell[29–31]. The two structures shown in Fig. 4 were optimized at the DFT level of theory using the B3LYP functional and the 6-311++G(2d,2p) basis set[32,33]. The geometry optimization was performed with the Gaussian 09 package[34].

The energies and transition moments of the core excited states of the bare ions and microsolvated clusters were computed with the Algebraic Diagrammatic Construction method for the polarization propagator[35] within the core-valence separation approximation[36–38] (CVS-ADC(2)x) as implemented in the Q-Chem package[39–42]. In the case of Cl^- the 6-311++G(3df,3pd) basis set[32,43] (excluding f functions) was used for all atoms, whereas in the case of K^+ we used the 6-311+G(2d,p) basis set[32,33] on all atoms, and two additional sets of s, p and d diffuse functions were added on K. In our calculations the core space comprises the 1s orbital of K^+ or Cl^-, whereas the remaining occupied orbitals are included in the valence space. We analyzed the core excited states by expanding the natural orbitals occupied by the excited electron (singly occupied natural orbitals, SONOs) of the microsolvated clusters in the basis of SONOs of the bare ions as in[23].

The final states following KLL resonant Auger decay of $K^+(H_2O)_6$ and $Cl^-(H_2O)_6$ were computed at the Configuration Interaction Singles (CIS) level using the Graphical Unitary Group Approach (GUGA) as implemented in the GAMESS-US package[45–47]. In order to account for the relaxation effects upon core ionization, we used a restricted open-shell Hartree-Fock reference wave function with a hole in the 2s orbital of both K^+ and Cl^-. We used the 6-311++G(2d,2p) basis set[32,33,43] on all atoms augmented with two sets of s, p, d diffuse functions in the case of K^+, and three sets of s, p, d diffuse functions in the case of Cl^-. The active space comprises the 2s and 2p orbitals of K/Cl with occupancy fixed to 6 and all virtual orbitals with occupancy fixed to 1. The remaining doubly occupied orbitals were frozen in the calculation.[48]

Acknowledgement

We thank Prof. Nobuhiro Kosugi and Dr. Matjaž Žitnik for the fruitful discussions. Experiments were performed at the GALAXIES beamline, SOLEIL Synchrotron, France (Proposal No. 20140160). The authors are grateful to the SOLEIL staff for assistance during the beam-

time. This project has received funding from the Research Executive Agency (REA) under the European Union's Horizon 2020 research and innovation programme Grant agreement No. 705515. Campus France and the PHC SIAM exchange program are acknowledged for financial support (project No. 38282QB). L. S. Cederbaum and N. V. Kryzhevoi acknowledge the financial support of the European Research Council (ERC) (Advanced Investigator Grant No. 692657) and the Deutsche Forschungsgemeinschaft (DFG research unit 1789).

Supporting Information Available

- suppinfo.pdf: contains 1) the radial density distributions of the core excited states of the bare ions; 2) partial cross sections and charge transfer time extracted from the experimental 2D map near the Cl 1s edge.

References

(1) Smith, J. W.; Saykally, R. J. Soft X-ray Absorption Spectroscopy of Liquids and Solutions. *Chem. Rev.* **2017**, *117*, 13909–13934, PMID: 29125751.

(2) O'Neill, P.; Stevens, D. L.; Garman, E. F. Physical and chemical considerations of damage induced in protein crystals by synchrotron radiation: a radiation chemical perspective. *J. Synchrotron Radiat.* **2002**, *9*, 329–332.

(3) Carugo, O.; Carugo, K. D. When X-rays modify the protein structure: radiation damage at work. *Trends Biochem. Sci.* **2005**, *30*, 213–219.

(4) Stumpf, V.; Gokhberg, K.; Cederbaum, L. S. The role of metal ions in X-ray-induced photochemistry. *Nat. Chem.* **2016**, *8*, 237–241.

(5) Stoychev, S. D.; Kuleff, A. I.; Tarantelli, F.; Cederbaum, L. S. On the interatomic

electronic processes following Auger decay in neon dimer. *J. Chem. Phys.* **2008**, *129*, 074307.

(6) Demekhin, P. V.; Scheit, S.; Stoychev, S. D.; Cederbaum, L. S. Dynamics of interatomic Coulombic decay in a Ne dimer following the $K{-}L_1L_{2,3}(^1P)$ Auger transition in the Ne atom. *Phys. Rev. A* **2008**, *78*, 043421.

(7) Demekhin, P. V.; Chiang, Y.-C.; Stoychev, S. D.; Kolorenč, P.; Scheit, S.; Kuleff, A. I.; Tarantelli, F.; Cederbaum, L. S. Interatomic Coulombic decay and its dynamics in NeAr following K-LL Auger transition in the Ne atom. *J. Chem. Phys.* **2009**, *131*, 104303.

(8) Ouchi, T.; Sakai, K.; Fukuzawa, H.; Higuchi, I.; Demekhin, P. V.; Chiang, Y.-C.; Stoychev, S. D.; Kuleff, A. I.; Mazza, T.; Schöffler, M. et al. Interatomic Coulombic decay following Ne 1s Auger decay in NeAr. *Phys. Rev. A* **2011**, *83*, 053415.

(9) Miteva, T.; Chiang, Y.-C.; Kolorenč, P.; Kuleff, A. I.; Cederbaum, L. S.; Gokhberg, K. The effect of the partner atom on the spectra of interatomic Coulombic decay triggered by resonant Auger processes. *J. Chem. Phys.* **2014**, *141*, 164303.

(10) Travnikova, O.; Marchenko, T.; Goldsztejn, G.; Jänkälä, K.; Sisourat, N.; Carniato, S.; Guillemin, R.; Journel, L.; Céolin, D.; Püttner, R. et al. Hard-X-Ray-Induced Multistep Ultrafast Dissociation. *Phys. Rev. Lett.* **2016**, *116*, 213001.

(11) Gokhberg, K.; Kolorenč, P.; Kuleff, A. I.; Cederbaum, L. S. Site- and energy-selective slow-electron production through intermolecular Coulombic decay. *Nature* **2014**, *505*, 661–663.

(12) Trinter, F.; Schöffler, M. S.; Kim, H.-K.; Sturm, F. P.; Cole, K.; Neumann, N.; Vredenborg, A.; Williams, J.; Bocharova, I.; Guillemin, R. et al. Resonant Auger decay driving intermolecular Coulombic decay in molecular dimers. *Nature* **2014**, *505*, 664–666.

(13) Pokapanich, W.; Bergersen, H.; Bradeanu, I. L.; Marinho, R. R. T.; Lindblad, A.; Legendre, S.; Rosso, A.; Svensson, S.; Björneholm, O.; Tchaplyguine, M. et al. Auger Electron Spectroscopy as a Probe of the Solution of Aqueous Ions. *J. Am. Chem. Soc.* **2009**, *131*, 7264–7271.

(14) Pokapanich, W.; Kryzhevoi, N. V.; Ottosson, N.; Svensson, S.; Cederbaum, L. S.; Öhrwall, G.; Björneholm, O. Ionic-charge dependence of the intermolecular Coulombic decay time-scale for aqueous ions probed by the core-hole clock. *J. Am. Chem. Soc.* **2011**, *133*, 13430.

(15) Unger, I.; Seidel, R.; Thürmer, S.; Pohl, M. N.; Aziz, E. F.; Cederbaum, L. S.; Muchová, E.; Slavíček, P.; Winter, B.; Kryzhevoi, N. V. Observation of electron-transfer-mediated decay in aqueous solution. *Nat. Chem.* **2017**, *9*, 708.

(16) Céolin, D.; Kryzhevoi, N. V.; Nicolas, C.; Pokapanich, W.; Choksakulporn, S.; Songsiriritthigul, P.; Saisopa, T.; Rattanachai, Y.; Utsumi, Y.; Palaudoux, J. et al. Ultrafast Charge Transfer Processes Accompanying KLL Auger Decay in Aqueous KCl Solution. *Phys. Rev. Lett.* **2017**, *119*, 263003.

(17) Russek, A.; Mehlhorn, W. Post-collision interaction and the Auger lineshape. *J. Phys. B At. Mol. Opt. Phys.* **1986**, *19*, 911.

(18) Guillemin, R.; Sheinerman, S.; Püttner, R.; Marchenko, T.; Goldsztejn, G.; Journel, L.; Kushawaha, R. K.; Céolin, D.; Piancastelli, M. N.; Simon, M. Postcollision interaction effects in KLL Auger spectra following argon $1s$ photoionization. *Phys. Rev. A* **2015**, *92*, 012503.

(19) Tchaplyguine, M.; Kivimäki, A.; Peredkov, S.; Sorensen, S. L.; Öhrwall, G.; Schulz, J.; Lundwall, M.; Rander, T.; Lindblad, A.; Rosso, A. et al. Localized versus delocalized excitations just above the 3d threshold in krypton clusters studied by Auger electron spectroscopy. *J. Chem. Phys.* **2007**, *127*, 124314.

(20) Sugiura, C. Influence of coordinating water on the chlorine K absorption spectra of hydrated metal dichlorides: MgCl2âŃĚ6H2O and SrCl2âŃĚ6H2O. *J. Chem. Phys.* **1982**, *77*, 681–682.

(21) Shadle, S. E.; Hedman, B.; Hodgson, K. O.; Solomon, E. I. Ligand K-edge x-ray absorption spectroscopic studies: metal-ligand covalency in a series of transition metal tetrachlorides. *J. Am. Chem. Soc.* **1995**, *117*, 2259–2272.

(22) Hertlein, M. P.; Adaniya, H.; Amini, J.; Bressler, C.; Feinberg, B.; Kaiser, M.; Neumann, N.; Prior, M. H.; Belkacem, A. Inner-shell ionization of potassium atoms ionized by a femtosecond laser. *Phys. Rev. A* **2006**, *73*, 062715.

(23) Miteva, T.; Wenzel, J.; Klaiman, S.; Dreuw, A.; Gokhberg, K. X-Ray absorption spectra of microsolvated metal cations. *Phys. Chem. Chem. Phys.* **2016**, *18*, 16671–16681.

(24) Céolin, D.; Marchenko, T.; Guillemin, R.; Journel, L.; Kushawaha, R. K.; Carniato, S.; Huttula, S.-M.; Rueff, J. P.; Armen, G. B.; Piancastelli, M. N. et al. Auger resonant-Raman study at the Ar K edge as probe of electronic-state-lifetime interferences. *Phys. Rev. A* **2015**, *91*, 022502.

(25) Winter, B.; Weber, R.; Widdra, W.; Dittmar, M.; Faubel, M.; Hertel, I. V. Full Valence Band Photoemission from Liquid Water Using EUV Synchrotron Radiation. *J. Phys. Chem. A* **2004**, *108*, 2625–2632.

(26) Céolin, D.; Ablett, J.; Prieur, D.; Moreno, T.; Rueff, J.-P.; Marchenko, T.; Journel, L.; Guillemin, R.; Pilette, B.; Marin, T. et al. Hard X-ray photoelectron spectroscopy on the {GALAXIES} beamline at the {SOLEIL} synchrotron. *J. Electron Spectrosc. Relat. Phenom.* **2013**, *190, Part B*, 188 – 192.

(27) Rueff, J.-P.; Ablett, J. M.; Céolin, D.; Prieur, D.; Moreno, T.; Balédent, V.; Lassalle-Kaiser, B.; Rault, J. E.; Simon, M.; Shukla, A. The GALAXIES beamline at the

SOLEIL synchrotron: inelastic X-ray scattering and photoelectron spectroscopy in the hard X-ray range. *J. Synchrotron Rad.* **2015**, *22*, 175–179.

(28) Winter, B.; Faubel, M. Photoemission from Liquid Aqueous Solutions. *Chem. Rev.* **2006**, *106*, 1176–1211, PMID: 16608177.

(29) Ohtaki, H.; Radnai, T. Structure and dynamics of hydrated ions. *Chem. Rev.* **1993**, *93*, 1157–1204.

(30) Soper, A. K.; Weckström, K. Ion solvation and water structure in potassium halide aqueous solutions. *Biophys. Chem.* **2006**, *124*, 180 – 191.

(31) Ma, H. Hydration structure of Na^+, K^+, F^-, and Cl^- in ambient and supercritical water: A quantum mechanics/molecular mechanics study. *Int. J. Quant. Chem.* **2014**, *114*, 1006–1011.

(32) Krishnan, R.; Binkley, J. S.; Seeger, R.; Pople, J. A. SelfâĂŘconsistent molecular orbital methods. XX. A basis set for correlated wave functions. *J. Chem. Phys.* **1980**, *72*, 650–654.

(33) Blaudeau, J.-P.; McGrath, M. P.; Curtiss, L. A.; Radom, L. Extension of Gaussian-2 (G2) theory to molecules containing third-row atoms K and Ca. *J. Chem. Phys.* **1997**, *107*, 5016–5021.

(34) Frisch, M. J.; Trucks, G. W.; Schlegel, H. B.; Scuseria, G. E.; Robb, M. A.; Cheeseman, J. R.; Scalmani, G.; Barone, V.; Mennucci, B.; Petersson, G. A. et al. Gaussian 09 Revision D.01. Gaussian Inc. Wallingford CT 2009.

(35) Schirmer, J. Beyond the random-phase approximation: A new approximation scheme for the polarization propagator. *Phys. Rev. A* **1982**, *26*, 2395–2416.

(36) Barth, A.; Schirmer, J. Theoretical core-level excitation spectra of N_2 and CO by a new polarisation propagator method. *J. Phys. B At. Mol. Opt. Phys.* **1985**, *18*, 867.

(37) Cederbaum, L. S.; Domcke, W.; Schirmer, J. Many-body theory of core holes. *Phys. Rev. A* **1980**, *22*, 206–222.

(38) Barth, A.; Cederbaum, L. S. Many-body theory of core-valence excitations. *Phys. Rev. A* **1981**, *23*, 1038–1061.

(39) Wenzel, J.; Wormit, M.; Dreuw, A. Calculating core-level excitations and x-ray absorption spectra of medium-sized closed-shell molecules with the algebraic-diagrammatic construction scheme for the polarization propagator. *J. Comp. Chem.* **2014**, *35*, 1900–1915.

(40) Wenzel, J.; Wormit, M.; Dreuw, A. Calculating X-ray Absorption Spectra of Open-Shell Molecules with the Unrestricted Algebraic-Diagrammatic Construction Scheme for the Polarization Propagator. *J. Chem. Theory Comput.* **2014**, *10*, 4583–4598.

(41) Wormit, M.; Rehn, D. R.; Harbach, P. H.; Wenzel, J.; Krauter, C. M.; Epifanovsky, E.; Dreuw, A. Investigating excited electronic states using the algebraic diagrammatic construction (ADC) approach of the polarisation propagator. *Mol. Phys.* **2014**, *112*, 774–784.

(42) Shao, Y.; Gan, Z.; Epifanovsky, E.; Gilbert, A. T.; Wormit, M.; Kussmann, J.; Lange, A. W.; Behn, A.; Deng, J.; Feng, X. et al. Advances in molecular quantum chemistry contained in the Q-Chem 4 program package. *Mol. Phys.* **2015**, *113*, 184–215.

(43) McLean, A. D.; Chandler, G. S. Contracted Gaussian basis sets for molecular calculations. I. Second row atoms, Z=11âĂŞ18. *J. Chem. Phys.* **1980**, *72*, 5639–5648.

(44) Krause, M. O.; Oliver, J. H. Natural widths of atomic K and L levels, Kα X-ray lines and several KLL Auger lines. *J. Phys. Chem. Ref. Data* **1979**, *8*, 329–338.

(45) Brooks, B. R.; Laidig, W. D.; Saxe, P.; Handy, N. C.; Schaefer III, H. F. The Loop-Driven Graphical Unitary Group Approach: A Powerful Method for the Variational Description of Electron Correlation. *Phys. Scr.* **1980**, *21*, 312.

(46) Brooks, B. R.; Schaefer, H. F. The graphical unitary group approach to the electron correlation problem. Methods and preliminary applications. *J. Chem. Phys.* **1979**, *70*, 5092–5106.

(47) Schmidt, M. W.; Baldridge, K. K.; Boatz, J. A.; Elbert, S. T.; Gordon, M. S.; Jensen, J. H.; Koseki, S.; Matsunaga, N.; Nguyen, K. A.; Su, S. et al. General atomic and molecular electronic structure system. *J. Comp. Chem.* **1993**, *14*, 1347–1363.

(48) Mosnier, J.-P.; Kennedy, E. T.; van Kampen, P.; Cubaynes, D.; Guilbaud, S.; Sisourat, N.; Puglisi, A.; Carniato, S.; Bizau, J.-M. Inner-shell photoexcitations as probes of the molecular ions CH^+, OH^+, and SiH^+: Measurements and theory. *Phys. Rev. A* **2016**, *93*, 061401.